Bull. Mater. Sci., Vol. 34, No. 5, August 2011, pp. 1069–1075. © Indian Academy of Sciences.

Conductivity and dielectric studies on $(Na_{0.4}Ag_{0.6})_2PbP_2O_7$ compound

HAIBADO MAHAMOUD*, B LOUATI, F HLEL and K GUIDARA
Laboratoire de L'Etat Solide, Faculté des Sciences, de Sfax, University of Sfax, 3031 Sfax, Tunisia

MS received 1 December 2010; revised 3 February 2011

Abstract. Electrical properties of the $(Na_{0.4}Ag_{0.6})_2PbP_2O_7$ compound were studied using complex impedance spectroscopy in the frequency range 200 Hz–5 MHz and temperature range (484–593 K). Combined impedance and modulus plots were used to analyse the sample behaviour as a function of frequency at different temperatures. Temperature dependence of d.c. and a.c. conductivity indicates that electrical conduction in the material is a thermally activated process. The frequency dependence of the a.c. conduction activation energy was found to obey a mathematical formula.

Keywords. Impedance spectroscopy; scaling; a.c. conductivity; modulus formalism; pyrophosphate.

1. Introduction

During the last few years, a number of efforts were made by researchers to find out new solids with high ionic conductivity for industrial applications, such as solid state batteries, fuel cells, sensors, etc (Mariappan *et al* 2005a). In this way, numerous phosphate materials are prepared and their ionic conductivity reported. Phosphate compounds with a monovalent cation and layer structures stand for family of phosphate with highest ionic conductivity (Daidouh *et al* 1997).

In the literature, many layered double phosphates of $A^I_2B^{II}P_2O_7$ formulation were studied with A = Na or Ag and B = Pb, Pd, Cu, Mn, Zn etc (Laligant 1992; Erragh *et al* 1995; Huang and Hwu 1998; Belharouak *et al* 2000; Dridi *et al* 2000, 2001). The bidimensional structures of these phosphates are characterized by the association of BO_m polyhedra and the P_2O_7 pyrophosphate groups in shape of ribbons. The mobile monovalent cations are located between ribbons.

In this work, we are going to present and discuss electrical and dielectrical properties of the $(Na_{0.4}Ag_{0.6})_2PbP_2O_7$ mixed diphosphate. We have already studied the structure of $NaAgPbP_2O_7$ compound (Makram *et al* 2010) which crystallizes in the triclinic system with space group $P\bar{1}$. That structure consists of $[Pb_2P_4O_{14}]^{4-}$ entities formed by the association of corner-shared PbO_5 and P_2O_7 groups. The monovalent cations (Na^+/Ag^+) occupy two types of sites S1 ($z = 1/4$) and S2 ($z = 0$). The Na^+ is located between $[Pb_2P_4O_{14}]^{4-}$ entities wherever Ag^+ is localized between alternating lamina.

*Author for correspondence (haibado_mahamoud@yahoo.fr)

2. Experimental

Synthesis of powder of $(Na_{0.4}Ag_{0.6})_2PbP_2O_7$ mixed diphosphate was carried out by the standard solid-state reaction techniques. Stoichiometric quantities of Na_2CO_3, $AgNO_3$ and $NH_4H_2PO_4$ were ground, mixed and progressively heated first to 473 K to eliminate NH_3, H_2O and CO_2 and then to 673 K.

The electrical measurements were performed using two-electrode configurations. The powder was pressed into a pellet of 8 mm diameter and 0·7 mm thickness. The a.c. conductivity was measured using a Tegam 3550 impedance analyser, in the temperature range, 484–593 K, measuring real and imaginary parts of the sample impedance in the frequency range 200 Hz–5 MHz.

3. Results and discussion

3.1 *Crystalline parameters*

X-ray powder diffractogram (figure 1) reveals that the synthesized compound crystallizes in the triclinic system with the space group $P\bar{1}$ and the refined unit cell parameters are $a = 5{\cdot}495$ (2) Å, $b = 6{\cdot}922$ (3) Å, $c = 9{\cdot}600$ (4) Å, $\alpha = 106{\cdot}04$ (3)°, $\beta = 96{\cdot}04$ (3)°, $\gamma = 109{\cdot}06$ (3)° and $V = 323{\cdot}9$ (2) Å^3.

3.2 *Impedance analysis*

The resistance and capacitance associated with the solids could be estimated using impedance spectroscopy. Bode plots of the $(Na_{0.4}Ag_{0.6})_2PbP_2O_7$ sample are presented in figures 2(a) and (b). They show dependence of the modulus and phase of the impedance, respectively vs frequency.

At higher frequencies, the observed shapes are typical of relaxation mechanisms expressed by the R-CPE_1 parallel circuits. At lower frequencies, electrode polarization effects transduced by constant-phase elements (CPE_2) are evidenced.

Figure 3 shows Nyquist plots (imaginary impedance Z'' vs real impedance Z') and the corresponding equivalent circuits of $(Na_{0.4}Ag_{0.6})_2PbP_2O_7$ compound at selective temperatures.

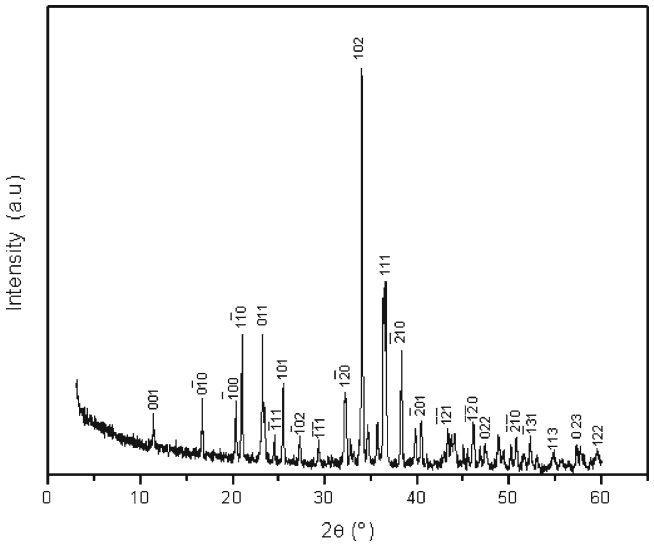

Figure 1. X-ray diffractogram of $(Na_{0.4}Ag_{0.6})_2PbP_2O_7$ in the 2θ range 5–60°.

The Nyquist plots confirm the suggestions given by the Bode plots. In the Z'' vs Z' plot, one observes a typical spectrum of the ionic conductors consisting of high frequency semicircle and low frequency tail. The intercept of the semicircles with the real axis gives the bulk resistance, R_b, excluding electrode polarization.

The expressions, which relate the modulus $|Z|$ and phase θ with frequency, are obtained from the real (Z') and imaginary part (Z'') of the complex impedance of the above circuit equivalent, as:

$$|Z| = \sqrt{Z'^2 + Z''^2},$$
$$\theta = \tan^{-1}\left(\frac{Z''}{Z'}\right),$$

where

$$Z' = \frac{R_b^2 Q_1 \omega^{\alpha_1} \cos(\alpha_1\pi/2) + R_b}{(1 + R_b Q_1 \omega^{\alpha_1} \cos(\alpha_1\pi/2))^2 + (R_b Q_1 \omega^{\alpha_1} \sin(\alpha_1\pi/2))^2} + \frac{\cos(\alpha_2\pi/2)}{Q_2\omega^{\alpha_2}}, \quad (1)$$

$$-Z'' = \frac{R_b^2 Q_1 \omega^{\alpha_1} \sin(\alpha_1\pi/2)}{(1+R_b Q_1 \omega^{\alpha_1} \cos(\alpha_1\pi/2))^2+(R_b Q_1 \omega^{\alpha_1} \sin(\alpha_1\pi/2))^2} + \frac{\sin(\alpha_2\pi/2)}{Q_2\omega^{\alpha_2}}. \quad (2)$$

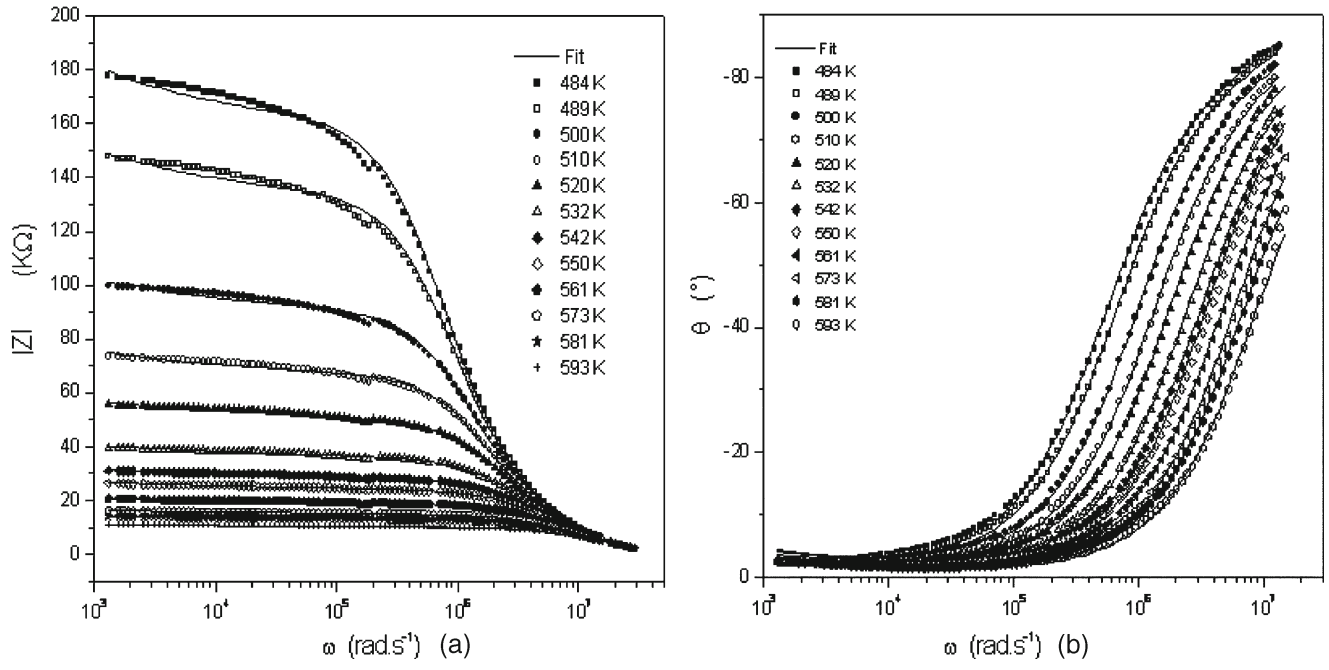

Figure 2. Bode plots for (**a**) $(Na_{0.4}Ag_{0.6})_2PbP_2O_7$: modulus of $|Z|$ vs frequency and **(b)** $(Na_{0.4}Ag_{0.6})_2PbP_2O_7$: phase θ vs frequency.

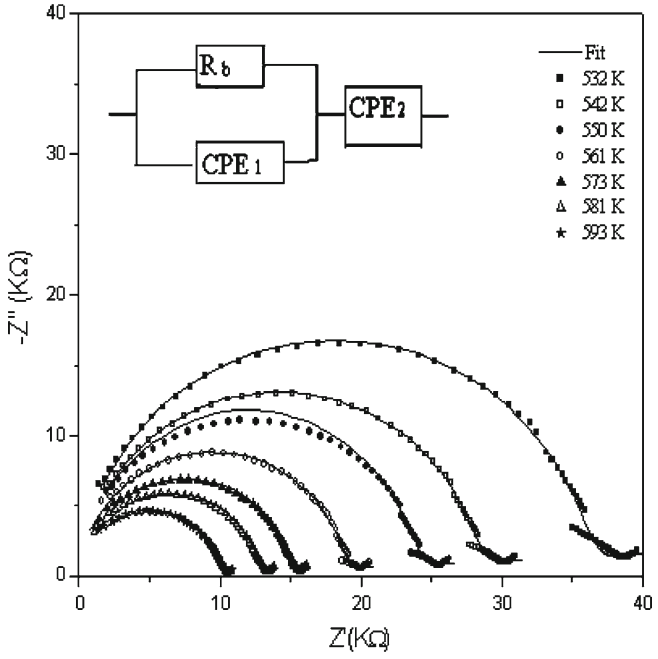

Figure 3. Nyquist plots (Z'' vs Z') for $(Na_{0.4}Ag_{0.6})_2PbP_2O_7$ with electrical equivalent circuit.

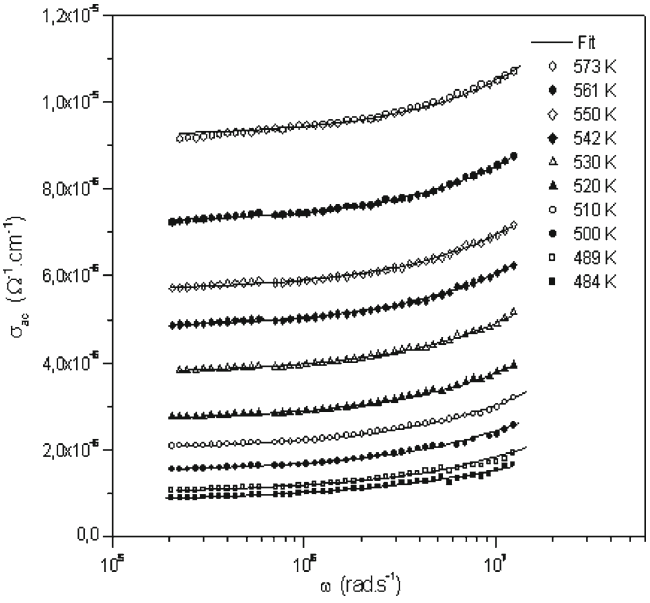

Figure 4. Frequency dependence of a.c. conductivity at some temperatures.

The magnitude of d.c. conductivity, σ_{dc}, can be calculated from R_b by the relation:

$$\sigma_{dc} = e/(R_b S),$$

where S is the electrolyte–electrode contact area and e the thickness of the sample. The bulk conductivity then obtained is found to be $8{\cdot}85 \times 10^{-6}$ S/cm at 573 K.

3.3 *Frequency dependent conductivity*

The conductivity representation is a most prominent representation to relate the macroscopic measurement to the microscopic movement of the ions. The a.c. conductivity has been calculated from the real and imaginary parts of the impedance data measured over a study range of temperatures. The frequency dependent conductivity spectrum is shown in figure 4 which displays a low frequency plateau and high frequency dispersive regions. The frequency independent conductivity characterizes the d.c. conductivity, due to the random diffusion of the ionic charge carriers via activated hopping. However, power-law dispersion indicates a non-random process wherein the ions perform correlated forward–backward motion (Mariappan *et al* 2005b). When the temperature increases, the transition from d.c. to the dispersive region shifts towards the higher frequency range. The conductivity, $\sigma_{ac}(\omega)$, is analysed using Jonscher's universal power law:

$$\sigma_{ac} = \sigma(0) + A\omega^s, \quad (3)$$

where $\sigma(0)$ is the d.c. conductivity, A a constant for a particular temperature. The frequency exponent s is related to the degree of correlation among moving ions and its value usually ranges between 0·6 and 1 for ion conducting materials (Jonscher 1983). He has shown that a non-zero s value in the dispersive region of conductivity is due to the energy stored in the short-range collective motion of ions. A higher s implies that large energy is stored in such collective motions (Jonscher 1983). Figure 5 shows the variation of A and s with temperature. One observes that the value of s increases linearly with temperature. This may be a result of the rise of the electrode polarization contribution with temperatures, which leads to decreasing amount of a.c. conductivity data available to perform the least-squares fitting.

A plot of $-\ln A$ vs s (inset of figure 5) indicates a linear temperature-independent and structure insensitive correlation between the values of these two parameters. Such behaviour was observed in different types of material and varied transport mechanism (Cramer *et al* 2003; Papathanassiou 2005a, b).

3.4 *Temperature-dependent conductivity*

D.c. electrical conductivity of the $(Na_{0.4}Ag_{0.6})_2PbP_2O_7$ evaluated from complex impedance spectrum data was observed as a function of temperature. Figure 6 shows the temperature dependence of the d.c. conductivity and hopping frequency. The pattern indicates an increase in conductivity with rise in temperature. This type of temperature dependence indicates

that the electrical conduction in the sample is a thermally activated transport process governed by Arrhenius type relation:

$$\sigma_{dc}T = \sigma_0 \exp(-E_a/kT),$$

where σ_0 $\left(\sigma_0 = 3{\cdot}53 \times 10^3 \Omega^{-1}.\mathrm{cm}^{-1}.K\right)$ is the d.c. conductivity pre-exponential factor and E_a the d.c. conductivity activation energy for mobile ions. The activation energy calculated from the slope of the $\ln(\sigma_{dc}T) = f(1000/T)$ is found to be 0·67 eV.

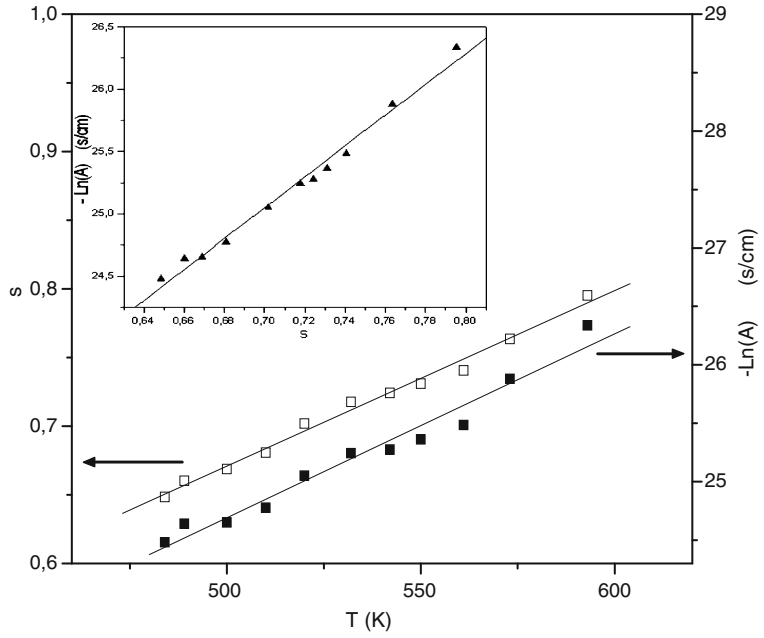

Figure 5. Variations of s and $-\ln(A)$ with temperature. In inset, correlation between $-\ln(A)$ and s is shown.

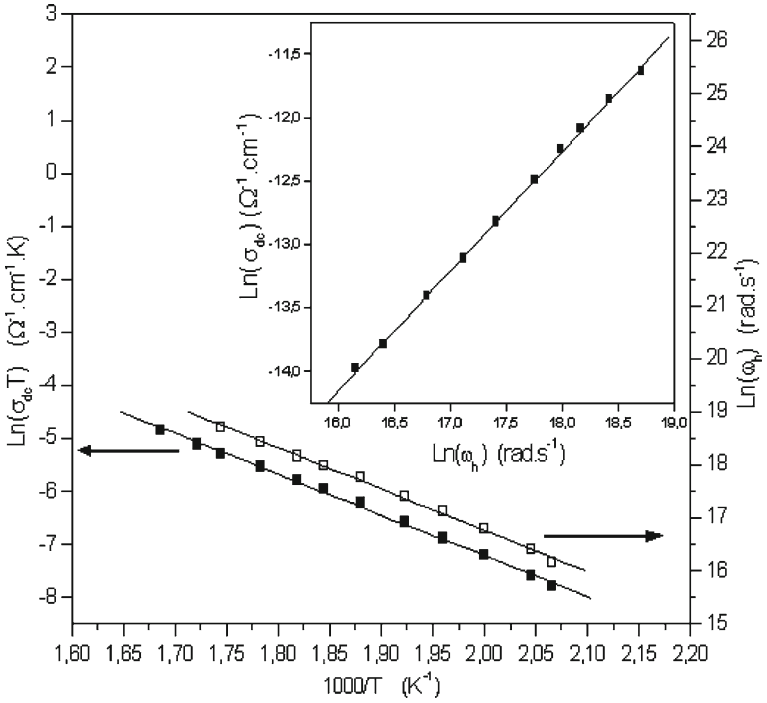

Figure 6. Temperature dependence of d.c. conductivity and hopping frequency. In inset, $\ln(\sigma_{dc})$ vs $\ln(\omega_h)$ is shown.

The crossover frequency from d.c. to the dispersive region of the a.c. conductivity is known as hopping frequency, ω_h and it can be calculated directly from a.c. conductivity data using the formula:

$$\omega_h = \left(\frac{\sigma\,(0)}{A}\right)^{1/s}. \tag{4}$$

Hopping frequency is temperature dependent and it obeys the Arrhenius equation:

$$\omega_h = \omega_0 \exp\left(-E_\omega/kT\right),$$

where ω_0 is the pre-exponential of hopping frequency and E_ω ($E_\omega = 0{\cdot}67$ eV) the activation energy for hopping frequency which is equal to the activation energy, E_a, determined above from d.c. conductivity.

In order to examine the correlation between a.c. and d.c. conduction, σ_{dc} values are plotted against ω_h (inset figure 6). The relation between $\ln(\sigma_{dc})$ and $\ln(\omega_h)$ shows a linear dependence with a slope value near to 1. This relation is analogous to the Barton–Nakajima–Namikawa (BNN) relation, $\sigma_{dc} \propto \omega_h$, where ω_h is the dielectric loss peak frequency (Mariappan and Govindaraj 2005). Hence, $\ln(\sigma_{dc})$ vs $\ln(\omega_h)$ plot with a slope of unity indicates that the d.c. and a.c. conductions are finely correlated in this sample.

A better way of displaying the frequency and temperature dependence of a.c. conductivity is to present the a.c. conductivity data in the form of Arrhenius plots at different frequencies. The temperature dependence of the a.c. conductivity is shown in figure 7. It is observed that the a.c. conductivity of the material increases with rise in temperature, and shows negative temperature coefficient of resistance behaviour. But it is worth noticing that the conductivity is found to be less temperature dependent at high frequency, i.e dispersive region. Moreover, the a.c. conductivity is found to be much less frequency dependent at high temperature. The activation energy, E_{ac} of σ_{ac} conductivity for selected frequency was determined from the slope of $\log \sigma_{ac}(\omega)T$ vs $1000/T$. The frequency variation of the obtained activation energy, E_{ac}, is shown in figure 8. It is clear that the value of a.c. conduction activation energy is constant and then it decreases with increasing frequency. This feature is fitted with the following expression (Soliman *et al* 2001):

$$E_{ac} = E_0\left(1 - \exp\left(-f_0/f\right)\right)^{\alpha}, \tag{5}$$

where E_0 is the d.c. activation energy at $f = 0$, f_0 ($f_0 =$ 158496 Hz) and α ($\alpha = 0{\cdot}06$) are the constants. It is clear from figure 8 that there is an excellent agreement between experimental and calculated curves.

3.5 *A.c. conductivity scaling*

The study of the frequency dependent conducting spectra of solids at different temperatures can be leading to a scaling law and it is called a time-temperature superposition principle (Dyre and Schrøder 2000). In the past few years, different scaling models have been proposed (Roling *et al* 1997; Sidebottom 1999; Ghosh and Pan 2000; Schroder and Dyre 2000). Figure 9 shows conductivity plots which are scaled

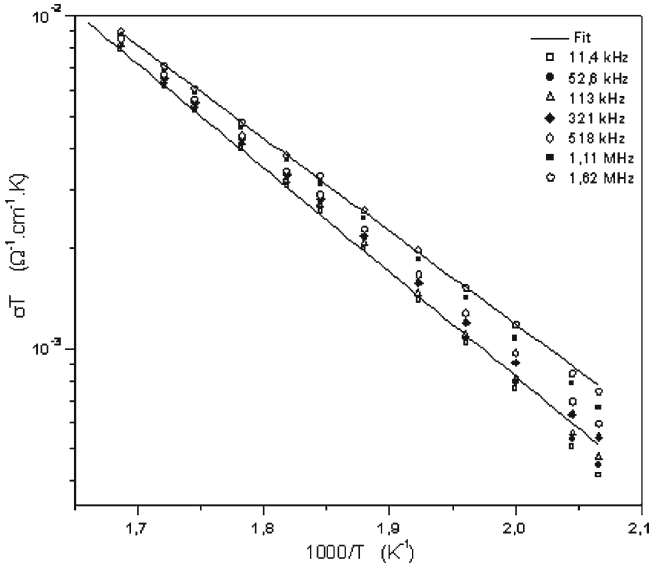

Figure 7. Plot of a.c. conductivity vs $1000/T$ at different frequencies.

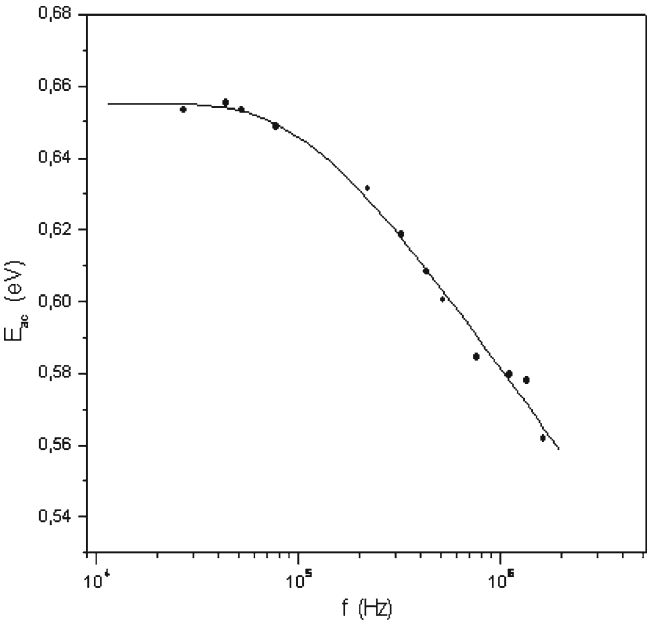

Figure 8. Frequency dependence of a.c. activation energy of conduction.

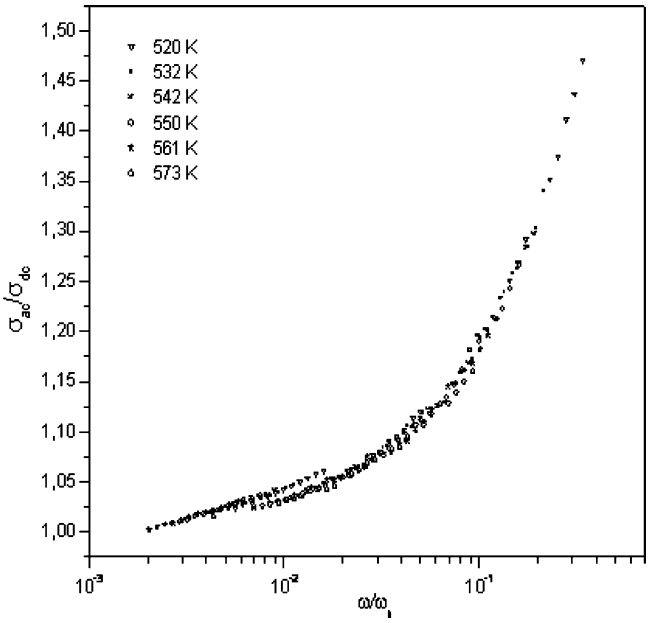

Figure 9. Plot of (σ/σ_{dc}) vs (ω/ω_h) at different temperatures.

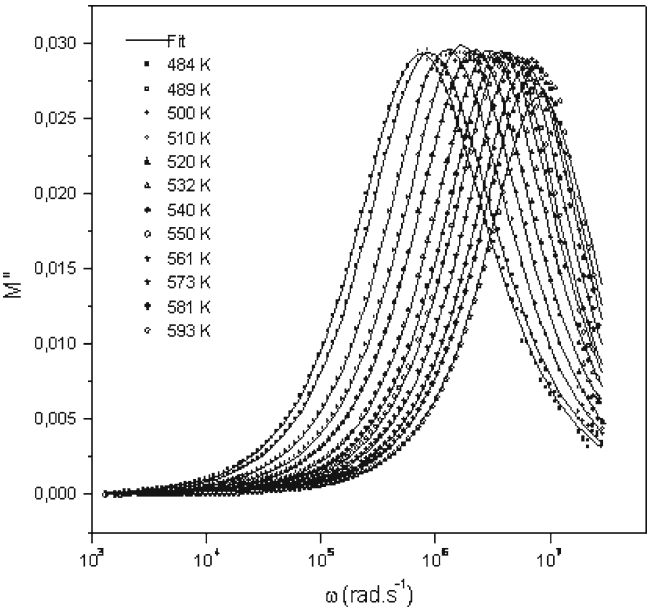

Figure 10. Frequency dependence of imaginary part of electric modulus at different temperatures.

using Ghosh formalism (Ghosh and Pan 2000; Mariappan and Govindaraj 2002). In this scaling process, the a.c. conductivity axis is scaled by σ_{dc} and the frequency axis by ω_h, σ_{dc} being a parameter obtained from power law fit. Scaling the conductivity spectra for $(Na_{0.4}Ag_{0.6})_2PbP_2O_7$ sample in this way at different temperatures merges on a single curve which implies that the relaxation dynamics of charge carriers is independent of temperature.

3.6 *Electric modulus analysis*

Electric modulus formalism is an important theory, formulated by Macedo *et al* (1972), which permits to study charge transport processes (such as mechanism of electrical transport, conductivity relaxation and ion dynamics as a function of frequency and temperature) in ion conductors and eliminates electrode polarization effect. The electric modulus (M^*) is calculated from the following equation:

$$M^*(\omega) = M' + jM'', \tag{6}$$

where $M' = \omega C_0 Z''$ and $M'' = \omega C_0 Z'$. Figure 10 shows the frequency dependence of the imaginary part of the electric modulus (M'') at different temperatures. The plot shows an asymmetric behaviour with respect to peak maxima whose positions are frequency and temperature dependent. These spectra also reflect the motions of the ions in the material by exhibiting two apparent relaxation regions. The left regions of the peak indicate the conduction process while regions on the right of the peak is associated to the relaxation process where the ion can make localized motion within the well.

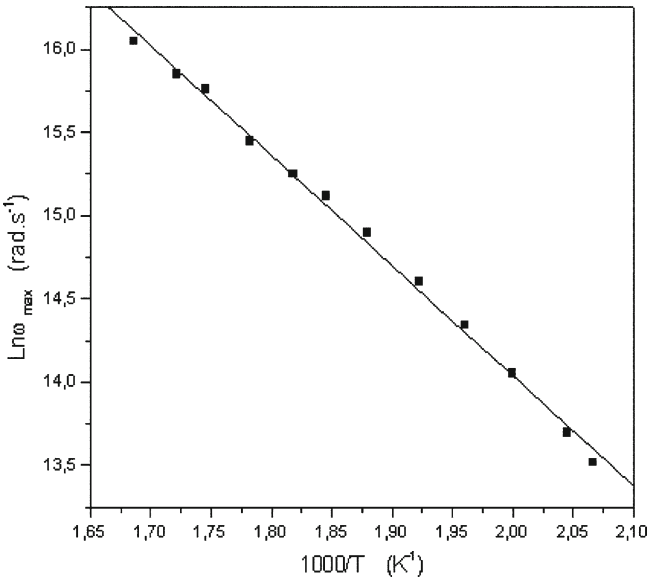

Figure 11. Arrhenius plot of $\ln(\omega_{max})$ vs $1000/T$.

The general method to check nature of the dielectric relaxation in the solid is to fit the measured data by Kohlrausch–Williams–Watts (KWW) decay function (Williams and Watts 1970). This function accounts for an asymmetric distribution of relaxation times resulting from a dielectric dispersion within a system through the exponential parameter, β. We have fitted the imaginary parts of the electric modulus for different temperatures with an approximate frequency representation of KWW function, proposed recently by Bergman

(Vinoth Rathan and Govindaraj 2010) and allowing a more direct and easy analysis in the frequency domain:

$$M'' = \frac{M''_{\max}}{1-\beta+\left[(\beta/(1+\beta))\left(\beta\,(\omega_{\max}/\omega)+(\omega/\omega_{\max})^{\beta}\right)\right]}, \tag{7}$$

where $M_{\max}$ and $\omega_{\max}$ are the peak maximum and peak frequency of imaginary part of the modulus, respectively. As shown in figure 10, the experimental data are well fitted to (7) and the parameters $M_{\max}$, ω_{m} and β were extracted from the analysis. The β value obtained lies in the range 0·8–1. Figure 11 shows the variation of relaxation frequency, $\omega_{\max}$ $(= 1/\tau_{\mathrm{p}})$ as a function of temperature. The plot obeys the Arrhenius nature and the activation energy calculated from linear regression is found to be 0·57 eV. This value is comparable to activation energy deduced from the impedance semicircles which suggest that the charge carrier has to overcome the same energy barrier while conducting as well as relaxing.

4. Conclusions

The complex plane impedance plots of the $(Na_{0.4}Ag_{0.6})_2PbP_2O_7$ compound, synthesized by the solid state reaction technique, show that the dielectric relaxation in this material is a bulk phenomenon. The a.c. conductivity spectra are found to obey Jonscher's universal power law with n varying between 0·64 and 0·80. The variation of the a.c. conduction activation energies with frequency was found to obey a mathematical formula. The activation energy calculated from modulus formalism spectra was consistent with the estimated value from impedance spectra, indicating that the ion has to overcome almost same energy barrier while conducting and relaxing. Finally, scaling analysis of the conductivity provides the time–temperature superposition principle on the ion dynamics in the material.

References

Belharouak I, Gravereau P, Parent C, Chaminade J P, Lebraud E and Le Flem G 2000 *J. Solid State Chem.* **152** 466

Cramer Z C, Brunklaus S, Ratai E and Gao Y 2003 *Phys. Rev. Lett.* **91** 266601

Daidouh A, Veiga M L, Marin C P and Martinez-Ripoll M 1997 *Acta Crystallogr.* **C53** 167

Dridi N, Boukhari A, Réau J M, Arbib E and Holt E M 2000 *Solid State Ionics* **127** 141

Dridi N, Boukhari A, Réau J M, Arbib E and Holt E M 2001 *Mater. Lett.* **47** 212

Dyre J C and Schrøder T B 2000 *Rev. Mod. Phys.* **72** 873

Erragh F, Boukhari A, Elouadi B and Abraham F 1995 *J. Solid State Chem.* **120** 23

Ghosh A and Pan A 2000 *Phys. Rev. Lett.* **84** 2188

Huang Q and Hwu S -J 1998 *Inorg. Chem.* **37** 5869

Jonscher A K 1983 *Dielectric relaxation in solids* (London: Chelsea Dielectric Press)

Laligant Y 1992 *Eur. J. Solid State Inorg. Chem.* **29** 83

Macedo P B, Moynihan C T and Bose R 1972 *Phys. Chem. Glasses* **13** 171

Makram M, Mahmoud H, Louati B, Hlel F and Guidara K 2010 *Ionics* **16** 655

Mariappan C R and Govindaraj G 2002 *Mater. Sci. Eng.* **B94** 82

Mariappan C R and Govindaraj G 2005 *Solid State Ionics* **176** 1311

Mariappan C R, Govindaraj G, Vinoth Rathan S and Vijaya Prakash G 2005a *Mater. Sci. Eng.* **B123** 63

Mariappan C R, Govindaraj G, Ramya L and Hariharan S 2005b *Mater. Res. Bull.* **40** 610

Papathanassiou A N 2005a *Mater. Lett.* **59** 1634

Papathanassiou A N 2005b *J. Phys. Chem. Solids* **66** 1849

Roling B, Happe A, Funke K and Ingram M D 1997 *Phys. Rev. Lett.* **78** 2160

Schroder T B and Dyre J C 2000 *Phys. Rev. Lett.* **84** 310

Sidebottom D L 1999 *Phys. Rev. Lett.* **82** 3653

Soliman M A, Reicha F M and Shaban A M 2001 *Polym. Bull.* **27** 311

Vinoth Rathan S and Govindaraj G 2010 *Mater. Chem. Phys.* **120** 255

Williams G and Watts D C 1970 *Trans. Faraday Soc.* **66** 80